APPLIED PHYSICS

Logic operations with active topological defects

Rui Zhang[1,2]*, Ali Mozaffari[1,4], Juan J. de Pablo[1,3]*

Logic operations performed by semiconductor-based transistors are the basis of modern computing. There is considerable interest in creating autonomous materials systems endowed with the capability to make decisions. In this work, we introduce the concept of using topological defects in active matter to perform logic operations. When an extensile active stress in a nematic liquid crystal is turned on, +1/2 defects can self-propel, in analogy to electron transport under a voltage gradient. By relying on hydrodynamic simulations of active nematics, we demonstrate that patterns of activity, when combined with surfaces imparting certain orientations, can be used to control the formation and transport of +1/2 defects. We further show that asymmetric high- and low-activity patterns can be used to create effective defect gates, tunnels, and amplifiers. The proposed active systems offer the potential to perform computations and transmit information in active soft materials, including actin-, tubulin-, and cell-based systems.

INTRODUCTION

Logic operations, such as AND gates and OR gates, provide the basis for computing. Semiconductor-based integrated circuits, which rely on electrons to perform such operations, are a cornerstone of modern technology. Over the past decade, important advances with soft materials have increased the interest and demand for soft robots and wearable electronic devices (*1*, *2*). These systems, however, are controlled with traditional electronic devices. In this work, we ask the question of whether active materials, such as biological filaments with motor proteins, can be reconfigured in a manner that allows them to perform logic operations and transmission of information. If possible, then these operations could be used for computing by the active material itself, helping to pave the way for development of soft materials systems capable of making decisions (*3*).

Nematic liquid crystals (LCs) consist of anisotropic molecules, which can flow similar to a liquid but exhibit a long-range orientational ordering (*4*). In regions where this orientational order is frustrated, topological defects emerge (*5*). These defects carry a topological charge and satisfy the Poincaré-Hopf theorem, which states that the total topological charge should be preserved (*6*). There are two types of LCs: one is thermotropic LC, which can enter nematic phase within certain temperature range, and the other is lyotropic LC, whose LC phases are controlled by both temperature and solute concentration. Recent studies have shown that defects in traditional thermotropic LCs, such as 4-cyano-4′-pentylbiphenyl (5CB), serve to sequester colloidal particles (*7*, *8*) and amphiphilic molecules (*9*, *10*) and can therefore be used as molecular carriers or nanoreactors. A growing trend of LC research has been the study of lyotropic, active LCs, in which local stresses are generated by the active motion of its constituents or components, which can give rise to collective dynamics, i.e., spontaneous flows and defect self-propulsion. Examples of active LCs include motor protein-driven biopolymer-based nematics (*11*, *12*), composites of swimming bacteria and nontoxic, passive LCs (*13*); the latter is also named living nematics (*14*). In the particular case of a two-dimensional (2D) active nematic, the comet-like +1/2 defects become motile. Because of its broken fore-aft symmetry, this type of defects can self-propel along their symmetry axis subjected to active stresses (*11*, *15*), and we propose to use active defects as information carriers in LCs. One can make an analogy between topological defects moving under active stresses and electron transport under a voltage gradient.

We envision that one possible application of topological defects is to provide a platform for the realization of logic operations. Past studies of defects in active nematics have been largely limited to their characterization (*16*–*22*). Attempts to control and manipulate defects have been limited in active systems (*23*–*25*), largely as a result of the challenges associated with preventing defect annihilations and harnessing the many-body interactions that arise among them. A notable exception is provided by a recent theoretical study that put forth the concept of storing information in +1/2 defects in a passive nematic material under the influence of an applied field (*26*).

In this work, we overcome these challenges by building on the concept of activity or stress patterning. The relevant experimental system is an actin-based 2D nematic LC (*12*, *27*). More specifically, rather than having a uniform activity throughout the entirety of the material, we introduce gradients of activity, as has been experimentally realized by gear-shifting light-sensitive myosin motors (*28*). Recent work using theory, simulation, and experiments has confirmed that +1/2 defects can be coerced to move along a given activity pattern (*29*, *30*). Independent theoretical works have discussed similar ideas (*31*, *32*). In comparison with the electronic circuits, the transport process in active nematic microfluidic systems is achieved through a spontaneous conversion of chemical energy of the medium into mechanical work.

Here, we build on that concept and demonstrate by hydrodynamic simulations that judicious design of high- and low-activity regions in microfluidic environments can lead to a high degree of control over +1/2 defect mobility. A key finding of our work is that the motion or "passage" of one defect can be facilitated or impeded by that of a second defect. We use these new concepts to realize defect gating, tunneling, and amplification by introducing different designs. Computations based on soft and biological systems have been considered in, for example, bacteria (*33*), slime mold (*34*, *35*), submillimeter bubbles (*36*, *37*), ferrofluid droplets (*38*), DNAs (*39*, *40*), and active fluid networks (*41*, *42*). The advantages of using

[1]Pritzker School of Molecular Engineering, University of Chicago, Chicago, IL 60637, USA. [2]Department of Physics, Hong Kong University of Science and Technology, Clear Water Bay, Kowloon, Hong Kong SAR. [3]Materials Science Division, Argonne National Laboratory, Argonne, IL 60439, USA. [4]OpenEye Scientific Software, Inc., 9 Bisbee Court Suite D, Santa Fe, New Mexico 87508, USA.
*Corresponding author. Email: ruizhang@ust.hk, (R.Z.); depablo@uchicago.edu(J.J.d.P.)

active topological defects as information carriers are that they can operate without the need for an external driving force, they can perform decentralized decision making, and they are topologically protected from noise, thereby providing an attractive, alternative candidate for soft matter–based logic operations. By demonstrating these elementary operations based on topological defects, we propose that combinations of these basic operations could enable defect redistribution, precise manipulation of optical properties, and autonomous transport in response to external cues, light in actin-based materials or nutrients in bacteria-based living nematics.

RESULTS

Our simulation is based on the Landau–de Gennes free energy functional (*4*). The microstructure of the nematic field, represented by a tensorial order parameter, namely, **Q**-tensor, is governed by the Beris-Edwards equation (*43*). A momentum equation is solved simultaneously to characterize the hydrodynamic flows induced by the active stresses. We adopted hybrid lattice Boltzmann method to solve these governing equations (*44*–*46*). Model details are summarized in Materials and Methods. This simulation method has been shown to provide an accurate representation of structure and dynamics in a wide range of active materials, including tubulin-based nematics, actin-based nematics, and bacterial-based living nematics (*12*, *27*, *46*, *47*). By choosing the mesogen length as the characteristic unit length, elastic constant $L \sim 1$ pN, and viscosity $\eta \sim 0.1$ Pa·s, a unit length scale can be mapped onto $\xi \approx 1$ μm, and a unit time scale corresponds to $\tau \approx 0.56$ s. In what follows, all numbers are expressed in terms of simulation units.

In the patterned active nematics we consider here, the nematic field is freely allowed to relax, leading to the motion of topological defects. Active stress is modeled as an additional stress term in the hydrodynamic equation, expressed as $\mathbf{\Pi} = -\alpha\mathbf{Q}$, where activity parameter α is spatially nonuniform (see Materials and Methods for more details). In our simulation, we consider extensile active nematics, with α being 0 and positive for regions outside and inside the activity pattern, respectively. This spatial pattern of activity is fixed. The collective effect of extensile active stresses drives the +1/2 defect to move toward its head (Fig. 1A), as has been experimentally characterized and theoretically elucidated (*11*, *15*, *48*, *49*). Our work will be based on this feature.

We first consider the case of low activity, where +1/2 defects are mobile, but no new defects are nucleated. Figure 1 shows that a local active region can guide +1/2 defect trajectories in an otherwise passive nematic, be it open (Fig. 1A) or closed (Fig. 1B). A +1/2 defect follows the activity pattern, instead of moving horizontally along its orientation or symmetry axis, as it would in a uniform activity nematic (Fig. 1A). Our results show that +1/2 defects prefer to stay within the active region. When active stress is spatially nonuniform, it can give rise to an additional local force, namely, $\mathbf{F} = -\nabla\alpha \cdot \mathbf{Q}$, at activity boundaries. When a +1/2 defect is approaching such boundary from a more active region, this force serves to repel it and, therefore, confine it within the activity pattern (*30*). This behavior has been confirmed in experiments of actin filaments and gear-shifting myosin motors (*29*). This result suggests that one can design activity patterns that alter +1/2 defect pathways, as demonstrated in Fig. 1 (B and C), where we consider a cross channel with normal anchoring condition. A defect-free, ground state is reached by preparing a uniform initial director field along a diagonal direction with respect to the cross. Two degenerate ground states are possible to arrive at, i.e., with nematic directors at the intersection connecting quadrants I and III and directors connecting quadrants II and IV. Experimentally, an external field such as electric, magnetic, or flow field during thermal quench can favor one degenerate state over the other. The phenomena we discuss here will be qualitatively the same for these two degenerate states. Therefore, in this work, without loss of generality, we only consider the nematic field connecting quadrants II and IV in what follows (Figs. 2, B and C, and 3). We find that a defect entering the cross intersection from the lower channel tends to move into the right channel (Fig. 1C and movie S1), which bears the least elastic energy once the defect enters (Fig. 1D). This preference can be changed by exclusively activating the upper channel (Fig. 1B and movie S2). A defect is forbidden from entering the left channel by this particular nematic field, as the elastic penalty to do so would be large if the +1/2 defect slid into it. The logic operations presented in what follows are based on the principle that +1/2 defects will follow the activity pattern.

Defects can also be manipulated in high-activity systems, where active turbulence is manifested. We first consider flat active-passive boundaries. Defects are found to be repelled by an activity interface and reside in the active side (Fig. 2A), consistent with our low-activity results. An "effective" homeotropic anchoring condition emerges at such an activity boundary, where the director on the passive side adopts a perpendicular orientation. To examine the anchoring effect in more detail, we also present results for a different geometry consisting of an active nematic surrounding a passive circular pattern (Fig. 2B). As the constantly distorting director field evolves, two +1/2 defects occasionally emerge within the circular region, a feature that is reminiscent of a passive nematic confined into a disk with homeotropic anchoring. The ratio of the interdefect distance l and the circle diameter D is measured to be $l/D \approx 0.6$, indicating that the effective anchoring strength $W \geq 5 \times 10^{-7}$ N/m. In another independent calculation, we fit the orientation angle for a flat activity boundary to a Boltzmann distribution and extract an effective anchoring strength $W = 5 \times 10^{-7}$ to 7×10^{-7} N/m (Fig. 2C), consistent with the result found in the circular geometry, which corresponds to weak anchoring in thermotropic LCs. These findings indicate that, by patterning activity, it is possible to create soft microfluidic channels with homeotropic anchoring, a property that is used throughout the rest of this manuscript. A possible physical mechanism of this effective anchoring can be understood by analyzing the behavior of −1/2 defects accumulated at activity boundaries in terms of their orientations. The calculation of activity gradient–induced local force shows that −1/2 defects with one of their branches pointing to the passive region are favored. This will impose an effective normal anchoring condition to the passive LC region (see the Supplementary Materials and fig. S1). A more comprehensive and rigorous study of anchoring effect will be conducted in a future work.

In what follows, we discuss the possible logic operations that activity patterning can enable. We first revisit the cross channel shown in Fig. 3. A single +1/2 defect can travel through it horizontally (movie S3), and in Fig. 1B, we showed that it can also pass through vertically. After the horizontal passage of a +1/2 defect, the nematic field at the intersection is fundamentally changed, and the passage of a second +1/2 defect from the bottom channel becomes impossible, unless the director field in the horizontal channels restores to its ground-state configuration. The +1/2 defect is found to roam around at the intersection and is unable to enter any branch

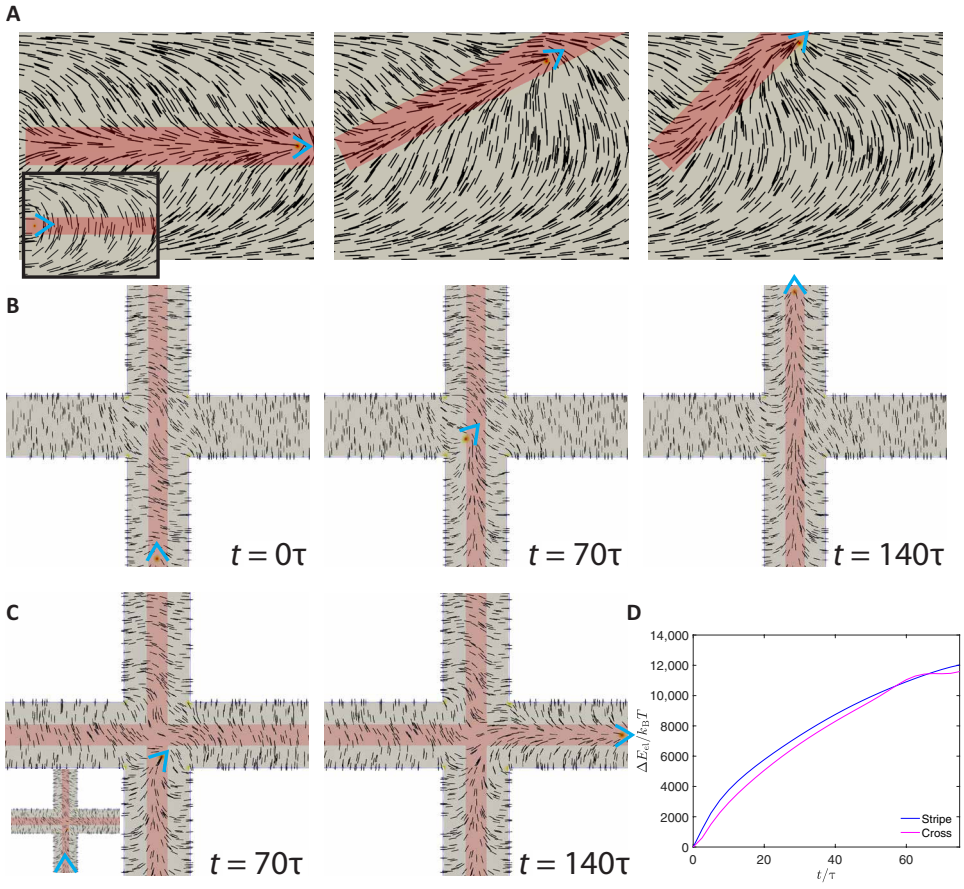

Fig. 1. Defect trajectory control via activity pattern. (**A**) A +1/2 defect follows a rectangular activity region (red shaded) with activity $\alpha = 0.002$. (**B**) +1/2 defect follows a vertical stripe of activity $\alpha = 0.0035$ and enters the top channel. (**C**) +1/2 defect chooses to enter the right channel under the influence of a cross pattern of activity $\alpha = 0.0035$. Inset shows the initial configuration similar to (B) at $t = 0$ τ. In (B) and (C), channel width is 60 and pattern width is 20. (**D**) Temporal elastic energy plot shows that defect entering the right channel for the cross pattern (C) is associated with entering a lower elastic energy state compared to the defect being forced into the upper channel for the stripe pattern (B).

Fig. 2. Anchoring effect at activity gradient boundary. (**A**) A slab of passive region of width 100 bound by active regions at activity level $\alpha = 0.002$. (**B**) A passive circular region with diameter 160 surrounded by active region exhibiting two +1/2 defects, reminiscent of a passive nematic confined in a cylinder with homeotropic anchoring. (**C**) Probability distribution function (pdf) of director orientations at various positions relative to the activity boundary ($x < 0$, passive region; $x > 0$, active region), showing the emergence of a homeotropic anchoring effect at the passive side of the boundary.

(Fig. 3 and movie S4). This finding indicates that it is possible to rely on one defect to control the dynamics or passage of another, thereby serving to facilitate more complex defect computations. Note that the passage of the first +1/2 defect has substantially raised the elastic energy of the system (Fig. 1D); thermal fluctuations are unable to destroy the information. However, an intruder −1/2 defect can erase this information and restore the initial director field. Our calculation shows that the passage time of a −1/2 defect on the same horizontal stripe pattern of activity is ~ 1106 τ, about eight times the passage time of a +1/2 defect, ~ 140 τ (Fig. 3A). This sets the time

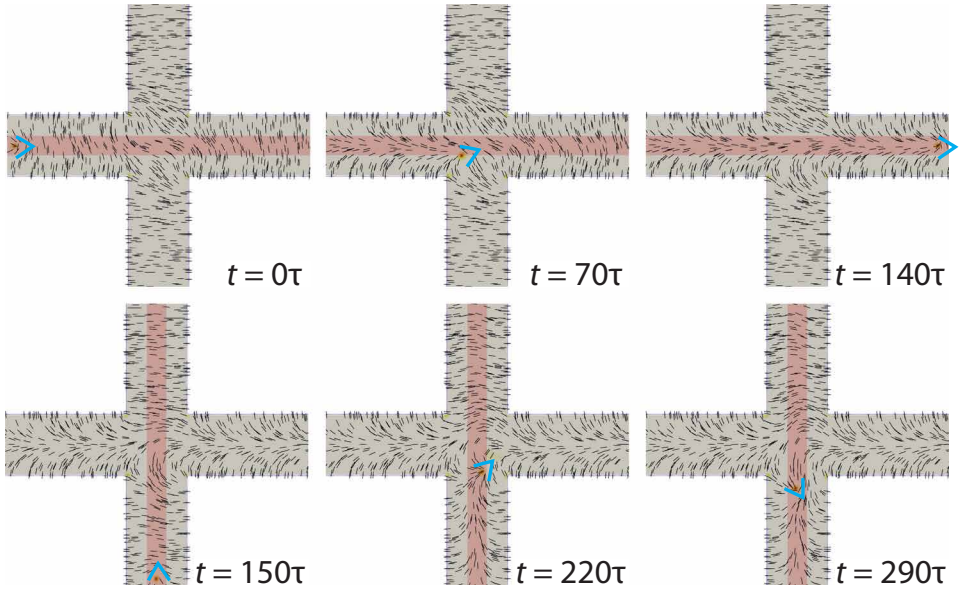

Fig. 3. Control of defect passage via a second defect. A +1/2 defect is sent from the left channel at $t = 0\ \tau$ with a horizontal stripe pattern of activity $\alpha = 0.0035$ and a second +1/2 defect is sent from the bottom channel with a vertical stripe pattern of activity $\alpha = 0.0035$ at $t = 150\ \tau$, when the first one has passed the intersection. This shows that the second defect is unable to pass the intersection. The channel width is 60 and the pattern width is 20.

scale that the passage of the first +1/2 defect can be remembered by the system. To protect this information, one has to turn off the pattern right after the passage.

Defect-based tunneling and gating operations, analogous to those found in transistors, can be performed by introducing asymmetric patterns. A triangular activity pattern, for example, can nucleate a ±1/2 defect pair from an otherwise uniform nematic (*29*). Here, we take advantage of this mechanism and create an array of closely spaced triangular patterns in a channel having an initial vertical nematic field. Activation of these triangular regions leads to formation of pairs of defects. The key feature here is that the newly generated −1/2 defect at each triangular pattern is subsequently annihilated by the approaching +1/2 defect coming from its left side. This gives rise to the instantaneous "tunneling" of a +1/2 defect over a long distance (Fig. 4A and movie S5). This process is reminiscent of electron transport in solids, where electrons move collectively, leading to their effective long-distance transport. The same triangular pattern can be used to realize defect gating. To this end, we consider two active regions (with activity level $\alpha = 0.001$) separated by a passive gap. Usually, the mobile +1/2 defect in one active region is unable to cross the gap and enter the other active region. This blockage can be overcome by introducing a high-activity triangular pattern. Similar to the defect tunneling idea, one can turn "on" a triangular high-activity pattern in the middle of the gap with activity level $\alpha = 0.022$, leading to the nucleation of a ±1/2 defect pair (Fig. 4B and movie S6). The awaiting +1/2 defect is then annihilated by the new −1/2 defect, which is left with a +1/2 defect on the other side that quickly escapes the gap. In the absence of the activity pattern, however, the awaiting defect is stuck at the gate (Fig. 4, C and D, and movie S6). Note that the time scale for this defect gating operation ($\approx 20\ \tau$) is much shorter than that associated with the active passage of defects without tunneling ($\approx 100\ \tau$; Fig. 4D). It takes $\sim 5\ \tau$ for the defect to tunnel the triangular pattern, but it has to spend $\sim 15\ \tau$ to pass the nonactive gaps between the activity pattern and the gate boundaries (Fig. 4D). Because the speed of isolated, self-propelling +1/2 defects is usually proportional to the activity level (*50*), the change in time scales, i.e., 5 τ against 100 τ, can be understood by the ratio of the activity levels in and outside the gate, i.e., $\alpha/\alpha' \approx 20$ (Fig. 4).

It is also possible to induce a defect-based "amplification" mechanism, analogous to that used in electronic systems where current or signals are amplified. Defects carry a topological charge, and their self-propulsion can also be regarded as a charge current. To demonstrate the concept of defect amplification, we consider two horizontal corridors connected by vertical channels (Fig. 5A and movie S7). The surfaces exhibit homeotropic anchoring, except at the top surface of the top corridor. The system is initially uniform but includes a +1/2 defect (shown in blue arrowheads) that is parked on the left side, i.e., the entrance of the bottom corridor. By following the horizontal activity pattern, the defect flows toward the right exit of the corridor, during which new +1/2 defects emerge from the channel corners and move into the top corridor following the vertical activity patterns. At the end of the process, when the original defect approaches the exit of the bottom corridor, all three generated defects (marked in yellow arrowheads) move into the top corridor. The new defects leave the corners before the original defect enters the junction, underscoring the fact that the interaction between the passing defect and the newly born defect exhibits a long-range elastic nature. Through additional design refinements of the channels at the top corridor, which are not shown here for brevity, it is possible to implement additional operations. Note that topological charge conservation still holds in this system. In Fig. 5B, we show the two director fields before and after the +1/2 defect nucleates from the corner. The effective topological charge of the surface defect at the corner is +1/4 (−1/4) before (after) the defect nucleation (*51*); the change in the topological charge at the corner thus gives rise to an additional +1/2 charge, preserving the total topological charge of the system. Note that, in this demonstration, amplification is 3×.

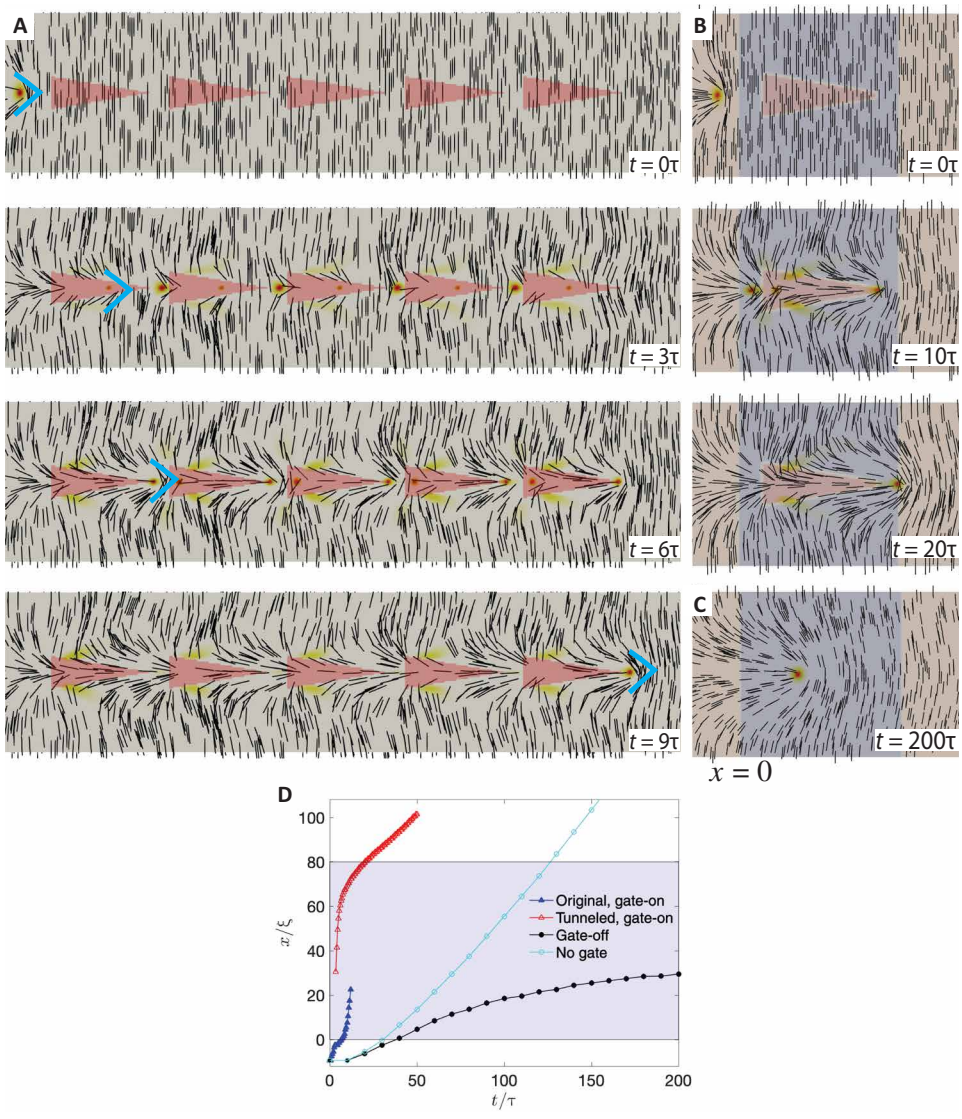

Fig. 4. Defect tunneling and gating. (**A**) A +1/2 defect is shown tunneling into the right side of a closely spaced array of triangular pattern with activity $\alpha = 0.022$. Each triangle has a base length of 18 and a height of 54. The channel width is 80. (**B**) Defect tunneling through a passive gap of width 80 via a triangular pattern of the same size and activity level as (A). (**C**) The +1/2 defect is unable to pass the gap after a sufficiently long time (100 τ). In (B) and (C), activity $\alpha' = 0.001$ is applied outside the gate to mobilize the defect. (**D**) Defect position as function of time for scenarios (B) and (C) and when there is no gate; the shadowed region indicates the gate region.

If we rely on micrometer-size actin-based nematics, then the theoretical amplification that can be achieved from a centimeter-scale device will be 1 cm/(10 ×1 μm) = O(10^3). However, if our experimental system is based on a low–molecular weight, thermotropic nematic, e.g., 5CB, whose characteristic defect size is 7 nm, then the theoretical amplification can reach to 1 cm/(10 × 7 nm) = O(10^5).

DISCUSSION

Here, we have shown that activity patterning provides a versatile and largely unexplored platform to manipulate the dynamics of +1/2 defects in a nematic LCs. Here, we have focused on 2D systems and examined defect passage through T-junctions and cross junctions. At modest activity levels, which are unable to nucleate new defects, different activity patterns can be used to guide defect trajectories. The interplay of active and elastic stresses gives rise to particular preferences for defect pathways. The passage of one defect can substantially change the director field at a junction, for example, and block the passage of a second defect coming from an orthogonal channel. At higher activity levels, a simple triangular pattern can nucleate a pair of ±1/2 defects in an otherwise uniform nematic. This phenomenon has been exploited to realize defect tunneling and gating. Last, we have demonstrated that it is possible to produce multiple defects out of an individual, passing defect to realize the concept of controlled defect amplification. In these demonstrations, the channel widths have been of order ~ 50 μm. Note that a homeotropic anchoring condition is generally needed because the +1/2 defect in a channel system must propel against a director field orthogonal to its symmetry axis.

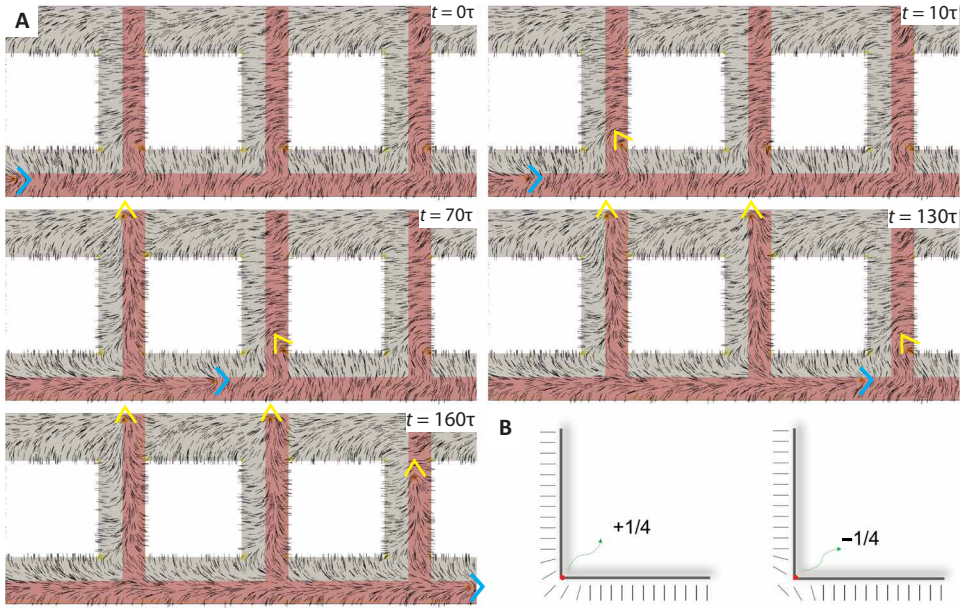

Fig. 5. Defect amplification. (**A**) Sequential snapshots of a +1/2 defect (marked in blue arrowheads) being sent into an otherwise defect-free system from the left end of the bottom corridor. New +1/2 defects are observed format each corner of the vertical channel when the original defect is approaching. Corridor and channel widths are 50, the activity pattern width is 25, and the activity level is $\alpha = 0.004$. (**B**) Schematics of the possible director fields near a corner before and after the nucleation of a +1/2 defect. The number indicates the effective topological charge of the corner defect.

Note that an alternative patterning active nematics can be realized by photopatterning local easy axis of a surface, which leads to a nematic with fixed director field (*52*). Bacteria swimming in such photopatterned nematics show intriguing patterns of dynamics (*14*, *53*). Surface patterning can also be realized using a smectic oil, which can provide an anisotropic environment and render the turbulent-like, active nematic flows into more ordered flows (*23*, *24*). More recently, a submersed micropatterned surface also demonstrates the capability of control over defect dynamics and spontaneous flows in microtubule-based active nematic film (*54*). We anticipate that our concept of activity patterning could be combined with these different patterning techniques and may lead to unprecedented phenomena and new applications.

We hope that the results presented here will stimulate new experimental work. Recent experiments have established that it is possible to pattern activity in experimental 2D actin systems using micromirror arrays and light-sensitive myosin motors. It should also be possible to pattern oxygen or nutrient concentrations in living LCs. Future work will extend the concepts and designs presented here to three dimensions, where preliminary results indicate that an even richer set of operations should be possible.

MATERIALS AND METHODS

Simulation method

Here, we detail the active nematodynamic equations and the numerical method adopted. The 2D nematic considered here is described by a nematic tensorial order parameter $\mathbf{Q}$ and a velocity field $\mathbf{u}$. For uniaxial nematics, the tensorial order parameter can be written as $\mathbf{Q} = S(\mathbf{nn} - \mathbf{I}/3)$, in which $\mathbf{n}$ is a unit vector representing the nematic field, S is the scalar order parameter of the nematic, and $\mathbf{I}$ is the identity tensor. By defining the strain rate field $\mathbf{D} = (\nabla\mathbf{u} + (\nabla\mathbf{u})^T)/2$ and the vorticity $\mathbf{\Omega} = (\nabla\mathbf{u} - (\nabla\mathbf{u})^T)/2$, one can introduce an advection term $\mathbf{S} = (\xi\mathbf{D} + \mathbf{\Omega})\cdot\left(\mathbf{Q} + \frac{\mathbf{I}}{3}\right) + \left(\mathbf{Q} + \frac{\mathbf{I}}{3}\right)\cdot(\xi\mathbf{D} - \mathbf{\Omega}) - 2\xi\left(\mathbf{Q} + \frac{\mathbf{I}}{3}\right)(\mathbf{Q}:\nabla\mathbf{u})$, where ξ is the flow-aligning parameter. The governing equation of the $\mathbf{Q}$-tensor, namely, the Beris-Edwards equation, can therefore be written as (*43*)

$$\frac{\partial\mathbf{Q}}{\partial t} + \mathbf{u}\cdot\nabla\mathbf{Q} - \mathbf{S} = \Gamma\mathbf{H} \tag{1}$$

where Γ is related to the rotational viscosity of the underlying nematic $\gamma_1 = 2S_0^2/\Gamma$ with S_0 being the equilibrium scalar order parameter (*55*), and $\mathbf{H}$ is the molecular field defined as $\mathbf{H} = -\left(\frac{\delta F}{\delta\mathbf{Q}} - \frac{\mathbf{I}}{3}\mathrm{Tr}\left(\frac{\delta F}{\delta\mathbf{Q}}\right)\right)$, which drives the system toward thermodynamic equilibrium with a free energy functional $F = \int_V f dV$, the integrand of which reads $f = \frac{A_0}{2}\left(1 - \frac{U}{3}\right)\mathrm{Tr}\,(\mathbf{Q}^2) - \frac{A_0 U}{3}\mathrm{Tr}\,(\mathbf{Q}^3) + \frac{A U_0}{4}(\mathrm{Tr}\,(\mathbf{Q}^2))^2 + \frac{L}{2}(\nabla\mathbf{Q})^2$. The phenomenological coefficient A_0 sets the energy scale, U controls the magnitude of the equilibrium scalar order parameter S_0 via $S_0 = \frac{1}{4} + \frac{3}{4}\sqrt{1 - \frac{8}{3U}}$ (*56*), and L is the elastic constant under one-constant approximation.

The local fluid density ρ and velocity $\mathbf{u}$ are governed by the generalized incompressible Navier-Stokes equations, modified by a frictional dissipative term

$$\rho\left(\frac{\partial}{\partial t} + \mathbf{u}\cdot\nabla\right)\mathbf{u} = \nabla\cdot\mathbf{\Pi} - \nu\mathbf{u} \tag{2}$$

The total asymmetric stress tensor $\mathbf{\Pi} = \mathbf{\Pi}^p + \mathbf{\Pi}^a$ is a sum of a passive and an active stress, and ν is a damping parameter setting the hydrodynamic screening length. The viscoelastic properties of thenematic are lumped in the passive stress, which is a sum of viscous and elastic terms. The passive stress is written as $\mathbf{\Pi}^p = 2\eta\mathbf{D} - P_0\mathbf{I} + 2\xi\left(\mathbf{Q} + \frac{\mathbf{I}}{3}\right)(\mathbf{Q}:\mathbf{H}) - \xi\mathbf{H}\cdot\left(\mathbf{Q} + \frac{\mathbf{I}}{3}\right) - \xi\left(\mathbf{Q} + \frac{\mathbf{I}}{3}\right)\cdot\mathbf{H} - \nabla\mathbf{Q}:\frac{\delta F}{\delta\nabla\mathbf{Q}} + \mathbf{Q}\cdot\mathbf{H} - \mathbf{H}\cdot\mathbf{Q}$. Here, η is the isotropic viscosity and

P_0 is the isotropic bulk pressure. The active stress $\mathbf{\Pi}^a = -\alpha\mathbf{Q}$, with $\alpha = \alpha(\mathbf{r})$ being a spatially varying activity parameter. A spontaneous flow can be generated when α or $\mathbf{Q}$ has spatial gradient, with $\alpha > 0$ for extensile systems and $\alpha < 0$ for contractile ones. We use a hybrid lattice Boltzmann method to solve the coupled governing partial differential equations (Eqs. 1 and 2) (*47*, *57*, *58*). We chose the following parameters throughout the 2D simulation: $A_0 = 0.1$, $L = 0.1$, $U = 3.5$ (giving $q \simeq 0.62$), $\eta = 1/3$, $\Gamma = 0.1$, $\xi = 0.7$, $\nu = 0.01$, an infinite homeotropic anchoring condition, and a no-slip velocity field at the channel boundaries. The active/passive interface (tanh profile) is of width of two lattice units.

SUPPLEMENTARY MATERIALS

Supplementary material for this article is available at https://science.org/doi/10.1126/sciadv.abg9060

REFERENCES AND NOTES

1. G. M. Whitesides, Soft robotics. *Angew. Chem. Int. Ed.* **57**, 4258–4273 (2018).
2. Z. Bao, X. Chen, Flexible and stretchable devices. *Adv. Mater.* **28**, 4177–4179 (2016).
3. R. Zhang, A. Mozaffari, J. J. de Pablo, Autonomous materials systems from active liquid crystals. *Nat. Rev. Mater.* **6**, 437–453 (2021).
4. P. de Gennes, J. Prost, *The Physics of Liquid Crystals* (Oxford Univ. Press, 1995).
5. M. Kleman, O. D. Lavrentovich, *Soft Matter Physics* (Springer, 2001).
6. R. D. Kamien, The geometry of soft materials: A primer. *Rev. Mod. Phys.* **74**, 953–971 (2002).
7. J. K. Whitmer, X. Wang, F. Mondiot, D. S. Miller, N. L. Abbott, J. J. de Pablo, Nematic-field-driven positioning of particles in liquid crystal droplets. *Phys. Rev. Lett.* **11**, 227801 (2013).
8. M. Rahimi, T. F. Roberts, J. C. Armas-Pérez, X. Wang, E. Bukusoglu, N. L. Abbott, J. J. de Pablo, Nanoparticle self-assembly at the interface of liquid crystal droplets. *Proc. Natl. Acad. Sci. U.S.A.* **112**, 5297–5302 (2015).
9. X. Wang, D. S. Miller, E. Bukusoglu, J. J. de Pablo, N. L. Abbott, Topological defects in liquid crystals as templates for molecular self-assembly. *Nat. Mater.* **15**, 106–112 (2016).
10. X. Wang, Y.-K. Kim, E. Bukusoglu, B. Zhang, D. S. Miller, N. L. Abbott, Experimental insights into the nanostructure of the cores of topological defects in liquid crystals. *Phys. Rev. Lett.* **116**, 147801 (2016).
11. T. Sanchez, D. T. N. Chen, S. J. De Camp, M. Heymann, Z. Dogic, Spontaneous motion in hierarchically assembled active matter. *Nature* **491**, 431–434 (2012).
12. N. Kumar, R. Zhang, J. J. de Pablo, M. L. Gardel, Tunable structure and dynamics of active liquid crystals. *Sci. Adv.* **4**, eaat7779 (2018).
13. S. Zhou, A. Sokolov, O. D. Lavrentovich, I. S. Aranson, Living liquid crystals. *Proc. Natl. Acad. Sci. U.S.A.* **111**, 1265–1270 (2014).
14. T. Turiv, R. Koizumi, K. Thijssen, M. M. Genkin, H. Yu, C. Peng, Q.-H. Wei, J. M. Yeomans, I. S. Aranson, A. Doostmohammadi, O. D. Lavrentovich, Polar jets of swimming bacteria condensed by a patterned liquid crystal. *Nat. Phys.* **16**, 481–487 (2020).
15. L. Giomi, M. J. Bowick, X. Ma, M. Cristina Marchetti, Defect annihilation and proliferation in active nematics. *Phys. Rev. Lett.* **110**, 228101 (2013).
16. M. C. Marchetti, J. F. Joanny, S. Ramaswamy, T. B. Liverpool, J. Prost, M. Rao, R. A. Simha, Hydrodynamics of soft active matter. *Rev. Mod. Phys.* **85**, 1143–1189 (2013).
17. A. Doostmohammadi, J. Ignés-Mullol, J. M. Yeomans, F. Sagués, Active nematics. *Nat. Commun.* **9**, 3246 (2018).
18. P. W. Ellis, D. J. G. Pearce, Y.-W. Chang, G. Goldsztein, L. Giomi, A. Fernandez-Nieves, Curvature-induced defect unbinding and dynamics in active nematic toroids. *Nat. Phys.* **14**, 85–90 (2018).
19. A. J. Tan, E. Roberts, S. A. Smith, U. A. Olvera, J. Arteaga, S. Fortini, K. A. Mitchell, L. S. Hirst, Topological chaos in active nematics. *Nat. Phys.* **15**, 1033–1039 (2019).
20. H. Li, X.-q. Shi, M. Huang, X. Chen, M. Xiao, C. Liu, H. Chaté, H. P. Zhang, Data-driven quantitative modeling of bacterial active nematics. *Proc. Natl. Acad. Sci.* **116**, 777–785 (2019).
21. G. Duclos, R. Adkins, D. Banerjee, M. S. E. Peterson, M. Varghese, I. Kolvin, A. Baskaran, R. A. Pelcovits, T. R. Powers, A. Baskaran, F. Tosch, M. F. Hagan, S. J. Streichan, V. Vitelli, D. A. Beller, Z. Dogic, Topological structure and dynamics of three-dimensional active nematics. *Science* **367**, 1120–1124 (2020).
22. S. Čopar, J. Aplinc, Ž. Kos, S. Žumer, M. Ravnik, Topology of three-dimensional active nematic turbulence confined to droplets. *Phys. Rev. X* **9**, 031051 (2019).
23. P. Guillamat, J. Ignés-Mullol, F. Sagués, Control of active liquid crystals with a magnetic field. *Proc. Natl. Acad. Sci.* **113**, 5498–5502 (2016).
24. P. Guillamat, J. Ignés-Mullol, F. Sagués, Taming active turbulence with patterned soft interfaces. *Nat. Commun.* **8**, 564 (2017).
25. A. Opathalage, M. M. Norton, M. P. N. Juniper, B. Langeslay, S. A. Aghvami, S. Fraden, Z. Dogic, Self-organized dynamics and the transition to turbulence of confined active nematics. *Proc. Natl. Acad. Sci.* **116**, 4788–4797 (2019).
26. Ž. Kos, J. Dunkel, Nematic bits and logic gates. arXiv:2008.13094 [cond-mat.soft] (30 August 2020).
27. R. Zhang, N. Kumar, J. L. Ross, M. L. Gardel, J. J. de Pablo, Interplay of structure, elasticity, and dynamics in actin-based nematic materials. *Proc. Natl. Acad. Sci.* **115**, E124–E133 (2018).
28. M. Nakamura, L. Chen, S. C. Howes, T. D. Schindler, E. Nogales, Z. Bryant, Remote control of myosin and kinesin motors using light-activated gearshifting. *Nat. Nanotechnol.* **9**, 693–697 (2014).
29. R. Zhang, S. A. Redford, P. V. Ruijgrok, N. Kumar, A. Mozaffari, S. Zemsky, A. R. Dinner, V. Vitelli, Z. Bryant, M. L. Gardel, J. J. de Pablo, Spatiotemporal control of liquid crystal structure and dynamics through activity patterning. *Nat. Mater.* **20**, 875–882 (2021).
30. A. Mozaffari, R. Zhang, N. Atzin, J. J. de Pablo, Defect spirograph: Dynamical behavior of defects in spatially patterned active nematics. *Phys. Rev. Lett.* **126**, 227801 (2021).
31. S. Shankar, M. C. Marchetti, Hydrodynamics of active defects: From order to chaos to defect ordering. *Phys. Rev. X* **9**, 041047 (2019).
32. X. Tang, J. V. Selinger, Alignment of a topological defect by an activity gradient. *Phys. Rev. E* **103**, 022703 (2021).
33. L. Tweedy, P. A. Thomason, P. I. Paschke, K. Martin, L. M. Machesky, M. Zagnoni, R. H. Insall, Seeing around corners: Cells solve mazes and respond at a distance using attractant breakdown. *Science* **369**, eaay9792 (2020).
34. A. Tero, S. Takagi, T. Saigusa, K. Ito, D. P. Bebber, M. D. Fricker, K. Yumiki, R. Kobayashi, T. Nakagaki, Rules for biologically inspired adaptive network design. *Science* **327**, 439–442 (2010).
35. A. Adamatzky, *Physarum Machines: Computers From Slime Mould* (World Scientific, 2010), vol. 74.
36. M. Prakash, N. Gershenfeld, Microfluidic bubble logic. *Science* **315**, 832–835 (2007).
37. M. J. Fuerstman, P. Garstecki, G. M. Whitesides, Coding/decoding and reversibility of droplet trains in microfluidic networks. *Science* **315**, 828–832 (2007).
38. G. Katsikis, J. S. Cybulski, M. Prakash, Synchronous universal droplet logic and control. *Nat. Phys.* **11**, 588–596 (2015).
39. L. M. Adleman, Molecular computation of solutions to combinatorial problems. *Science* **266**, 1021–1024 (1994).
40. R. J. Lipton, Dna solution of hard computational problems. *Science* **268**, 542–545 (1995).
41. H. Wioland, F. G. Woodhouse, J. Dunkel, R. E. Goldstein, Ferromagnetic and antiferromagnetic order in bacterial vortex lattices. *Nat. Phys.* **12**, 341–345 (2016).
42. F. G. Woodhouse, J. Dunkel, Active matter logic for autonomous microfluidics. *Nat. Commun.* **8**, 15169 (2017).
43. A. N. Beris, B. J. Edwards, *Thermodynamics of Flowing Systems with Internal Microstructure* (Oxford Univ. Press Inc., New York and Oxford, 1994).
44. C. Denniston, D. Marenduzzo, E. Orlandini, J. M. Yeomans, Lattice boltzmann algorithm for three–dimensional liquid-crystal hydrodynamics. *Phil. Trans. R. Soc. Lond. A* **362**, 1745–1754 (2004).
45. D. Marenduzzo, E. Orlandini, M. E. Cates, J. M. Yeomans, Steady-state hydrodynamic instabilities of active liquid crystals: Hybrid lattice boltzmann simulations. *Phys. Rev. E* **76**, 031921 (2007).
46. R. Zhang, Y. Zhou, M. Rahimi, J. J. de Pablo, Dynamic structure of active nematic shells. *Nat. Commun.* **7**, 13483 (2016).
47. A. Sokolov, A. Mozaffari, R. Zhang, J. J. de Pablo, A. Snezhko, Emergence of radial tree of bend stripes in active nematics. *Phys. Rev. X* **9**, 031014 (2019).
48. F. C. Keber, E. Loiseau, T. Sanchez, S. J. De Camp, L. Giomi, M. J. Bowick, M. Cristina Marchetti, Z. Dogic, A. R. Bausch, Topology and dynamics of active nematic vesicles. *Science* **345**, 1135–1139 (2014).
49. X. Tang, J. V. Selinger, Theory of defect motion in 2D passive and active nematic liquid crystals. *Soft Matter* **15**, 587–601 (2019).
50. S. P. Thampi, R. Golestanian, J. M. Yeomans, Velocity correlations in an active nematic. *Phys. Rev. Lett.* **111**, 118101 (2013).
51. B. Senyuk, Q. Liu, Y. Yuan, I. I. Smalyukh, Edge pinning and transformation of defect lines induced by faceted colloidal rings in nematic liquid crystals. *Phys. Rev. E* **93**, 062704 (2016).
52. Y. Guo, M. Jiang, C. Peng, K. Sun, O. Yaroshchuk, O. Lavrentovich, Q.-H. Wei, High-resolution and high-throughput plasmonic photopatterning of complex molecular orientations in liquid crystals. *Adv. Mater.* **28**, 2353–2358 (2016).
53. C. Peng, T. Turiv, Y. Guo, Q.-H. Wei, O. D. Lavrentovich, Command of active matter by topological defects and patterns. *Science* **354**, 882–885 (2016).
54. K. Thijssen, D. A. Khaladj, S. Ali Aghvami, M. A. Gharbi, S. Fraden, J. M. Yeomans, L. S. Hirst, T. N. Shendruk, Submersed micropatterned structures control active nematic flow, topology, and concentration. *Proc. Natl. Acad. Sci. U.S.A.* **118**, e2106038118 (2021).
55. C. Denniston, E. Orlandini, J. M. Yeomans, Lattice boltzmann simulations of liquid crystal hydrodynamics. *Phys. Rev. E* **63**, 056702 (2001).

56. M. Ravnik, S. Žumer, Landau–de gennes modelling of nematic liquid crystal colloids. *Liq. Crys.* **36**, 1201–1214 (2009).
57. D. Marenduzzo, E. Orlandini, J. M. Yeomans, Interplay between shear flow and elastic deformations in liquid crystals. *J. Chem. Phys.* **121**, 582–591 (2004).
58. R. Zhang, T. Roberts, I. Aranson, J. J. de Pablo, Lattice boltzmann simulation of asymmetric ow in nematic liquid crystals with finite anchoring. *J. Chem. Phys.* **14**, 084905 (2016).

Acknowledgments
Funding: This work is supported by the National Science Foundation, under the University of Chicago MRSEC grant DMR-2011854, from the Division of Materials Science and Engineering. R.Z. also acknowledges financial support from Hong Kong Research Grants Council by grant no. 26302320. **Author contributions:** J.J.d.P. initiated and supervised the research. R.Z., A.M., and J.J.d.P. performed the research, analyzed the data, and wrote the paper. **Competing interests:** The authors declare that they have no competing interests. **Data and materials availability:** All data needed to evaluate the conclusions in the paper are present in the paper and/or the Supplementary Materials. Additional data are stored at https://doi.org/10.7910/DVN/GMY0HA.

Submitted 1 March 2021
Accepted 30 December 2021
Published 23 February 2022
10.1126/sciadv.abg9060

ScienceAdvances

Logic operations with active topological defects

Rui ZhangAli MozaffariJuan J. de Pablo

Sci. Adv., 8 (8), eabg9060. • DOI: 10.1126/sciadv.abg9060